Multiple sources of signaling noise in bacterial chemotaxis network

R. Colin[1,*,+], C. Rosazza[1,*], A. Vaknin[2], V. Sourjik[1,+]

[1]Max Planck Institute for Terrestrial Microbiology and LOEWE Center for Synthetic Microbiology (SYNMIKRO), Karl-von-Frisch-Strasse 16, D-35043 Marburg, Germany

[2] The Racah Institute of Physics, the Hebrew University, Jerusalem 91904, Israel

[*] Authors contributed equally to this work.

[+] Corresponding authors: victor.sourjik@synmikro.mpi-marburg.mpg.de,

remy.colin@synmikro.mpi-marburg.mpg.de

Abstract

Due to their relatively small size and a limited number of components, cells are intrinsically subject to stochastic fluctuations. Whereas stochasticity in gene expression has been extensively investigated, much less is known about posttranslational noise arising from activity fluctuations within protein networks. The pathway controlling chemotaxis of *Escherichia coli* provides one of the few examples where signaling noise has been previously deduced from cellular behavior. Here we use direct single-cell FRET measurements of the pathway activity to directly confirm the existence of signaling noise in chemotaxis and to characterize its determinants. Our analysis confirms previously proposed role of chemoreceptor methylation enzymes as major contributors to the pathway noise. However, it also demonstrates that allosteric interactions and slow receptor rearrangements within clusters of chemoreceptors contribute largely to activity fluctuations. Resulting mathematical description of activity fluctuations illustrates the inherent relation between the noise in the signaling system and its sensitivity to perturbations.

Introduction

It is well established that cellular processes are prone to fluctuations due to their intrinsic stochasticity combined with a small number of reactant molecules [1-3]. Best-characterized examples of such cellular noise relate to the variability in expression of genes or proteins, observed either across a population of genetically identical cells or within one cell over time [4, 5]. Such stochastic variability may be further enhanced by feedbacks present in gene regulatory networks, in extreme cases causing genetically identical cells to exhibit distinctly different behaviors [6-8]. In most cases the effects of noise are detrimental, limiting the ability of cellular networks to precisely perform such functions as information processing [1, 9-12]. Therefore, cellular networks are believed to have evolved features that enable them to function robustly in presence of stochastic fluctuations in the levels of their components [13-16].

In contrast to gene expression noise, much less is known about the origins, extent or effects of noise that can arise at the posttranslational level, although such noise is expected to be ubiquitous. Chemotaxis of *Escherichia coli*, a bacterial model for signal transduction, previously provided one of the few examples where signaling noise within the network has been indeed deduced from studies of cell motility and flagellar rotation [17-23]. Subsequent theoretical analysis suggested that such behavioral fluctuations might provide physiological benefit, by enhancing environmental exploration [18, 24-28].

At the molecular level, these fluctuations were proposed to originate within the methylation-based adaptation system [17, 29, 30]. Adaptation in chemotaxis is mediated by two enzymes, the methyltransferase CheR and the methylesterase CheB, which respectively add or remove methyl groups at four specific glutamate residues of the chemoreceptors [31-35]. Notably, for the major

chemoreceptors of *E. coli*, Tar and Tsr, two of these residues are initially encoded as glutamines that are functionally similar to methylated glutamates and subsequently deamidated to glutamates by CheB [35, 36]. Changes in receptor methylation control the activity of the sensory complexes which further include the receptor-associated kinase CheA and the scaffold protein CheW, such that methylation compensates effects of chemotactic stimulation via negative feedback loops [37-40]. This adaptation enables cells to robustly maintain intermediate CheA activity and thus intermediate phosphorylation of the response regulator CheY. Phosphorylated CheY (CheY-P) controls the rotation of flagellar motor and cell swimming. The adapted level of CheY-P falls into the most sensitive part of the motor response [41], ensuring that bacteria remains chemotactic in a wide range of background stimulation.

Despite this importance of the adaptation system for robust maintenance of the average signaling output, the relatively small number of methylation enzymes [42] and their slow exchange rates at their receptor substrates [43, 44] may result in fluctuations of the level of phosphorylated CheY [17, 18, 20]. Further amplified by the cooperative response of flagellar motor [29, 41], these fluctuations were suggested to produce the observed large variation in the motor rotation [18, 23] and in the swimming behavior [17, 45] of individual cells over time.

Besides amplification at the motor level, signals in the chemotaxis pathway are also amplified by cooperative interactions in signaling arrays (clusters) of chemoreceptors [46, 47]. These interactions have been previously described using either the Monod-Wyman-Changeux (MWC) model which assumes that receptors operate in units (signaling teams) of 10-20 dimers where activities of individual receptors are tightly coupled [48-50] or using an Ising model of a receptor lattice with intermediate coupling [51]. But despite the established importance of these

cooperative interactions for signal processing, the contribution of receptor clustering to the pathway noise remained untested.

Here we directly monitored signaling noise in *E. coli* chemotaxis pathway using Förster (fluorescence) resonance energy transfer (FRET). Combining single-cell experiments with mathematical analysis, we show that pathway activity fluctuations arise from interplay of multiple factors. Besides the methylation system, these include previously observed slow rearrangements within receptor clusters [52] as well as the cooperative interactions between clustered chemoreceptors.

Results

Pathway activity fluctuations in adapting cells

To perform time-resolved characterization of the chemotaxis pathway activity in individual *E. coli* cells, we adapted the microscopy-based ratiometric FRET assay that was previously used at the population level [53] . This assay relies on the phosphorylation-dependent interaction between CheY, fused to yellow fluorescent protein (CheY-YFP), and its phosphatase CheZ, fused to cyan fluorescent protein (CheZ-CFP). Whereas previous measurements of this FRET reporter relied on the signal collection from an area containing several hundred cells using photon counters [54], here we used imaging with the electron multiplication charge-coupled device (EM-CCD) camera (see Material and Methods). When integrated over the population, the chemoattractant response of *E. coli* cells that express the FRET pair and a major chemoreceptor Tar (Figure 1A) was very similar to the one observed previously [53, 55]. Upon stimulation with the chemoattractant α-methyl-aspartate (MeAsp) the ratio of the YFP to CFP fluorescence

92 decreased, consistent with the attractant-mediated inhibition of the kinase activity, and therefore
93 of energy transfer from the donor (CFP) to the acceptor (YFP). Furthermore, the pathway
94 subsequently adapted to the new background level of attractant via the CheR-dependent increase
95 in receptor methylation, but as previously reported adaptation to high levels of MeAsp is only
96 partial [55-57]. Subsequent removal of attractant resulted in a transient increase in kinase
97 activity, followed by the CheB-mediated adaptation through the demethylation of receptors.
98 Although the YFP/CFP ratio measured for individual cells during the same experiment was
99 expectedly noisier than the population-averaged data, both the initial response and subsequent
100 adaptation were clearly distinguishable (Figure 1B). In contrast to the population measurement,
101 however, a majority of individual cells also exhibited large fluctuations in the YFP/CFP ratio
102 (also Figure 1 – Figure Supplement 1), which were apparently different from the measurement
103 noise that was observed in the negative control (receptorless cells with largely inactive pathway;
104 Figure 1 – Figure Supplement 2). For cells adapted in buffer, these fluctuations could be as large
105 as the response to attractant. Importantly, these long-term fluctuations were initially suppressed
106 upon saturating inhibition of the pathway activity with 10 μM MeAsp but then (partly) recovered
107 upon (imperfect) adaptation, confirming their relation to the pathway activity.
108 To analyze these fluctuations in greater detail, the power spectral density (PSD) of the single-cell
109 YFP/CFP ratio, $s_R(\omega)$, was computed for buffer- or attractant-adapted cells, as well as for the
110 receptorless cells that do not activate CheA. The PSD enables to extract the average spectral
111 content of the temporal variations of the single-cell ratio, *i.e.* to determine frequencies at which
112 this ratio fluctuates. To rule out possible effects of the initial state of receptor modification on the
113 observed fluctuations, we analyzed cells that express Tar in either the native half-modified
114 (Tar^{QEQE}) state or in the unmodified (Tar^{EEEE}) state. We observed that at high frequency the PSD

kept a constant value independent of the condition or strain (Figure 1C), indicating that in this frequency range the shot noise of the measurements sets the lower bound of measurable kinase activity fluctuations. For the chemotactic cells adapted in buffer, the measured PSD increased dramatically at lower frequency (roughly as $1/\omega$), reaching a low frequency plateau at 0.015 Hz. Cells expressing Tar^{EEEE} or Tar^{QEQE} showed essentially identical behavior. Similar increase of the PSD at low frequency was observed for cells adapted to either 10 or 25 μM MeAsp, although the amplitude of this increase was smaller than for the buffer-adapted cells. In contrast, the receptorless strain showed nearly constant noise level over the entire frequency range.

The PSD was further used to calculate the average time autocorrelation function of the single-cell ratio (Figure 1D), which reflects the characteristic time scale of activity fluctuations. For cells adapted in buffer, the autocorrelation time constant was 9.5 ± 0.5 s (as determined by a single exponential fit of the correlation function), which is similar to the characteristic time of the pathway activity fluctuation previously deduced from behavioral studies [17, 22]. Same characteristic time was observed in the MeAsp-adapted cells, although the amplitude of the correlation was considerably smaller in this case. Interestingly, on the longer time scale the autocorrelation function becomes weakly negative, indicating an overshoot that is likely caused by the negative feedback in the adaptation system [58]. No autocorrelation was observed for the receptorless cells, again confirming that the autocorrelation is due to fluctuations of the pathway activity.

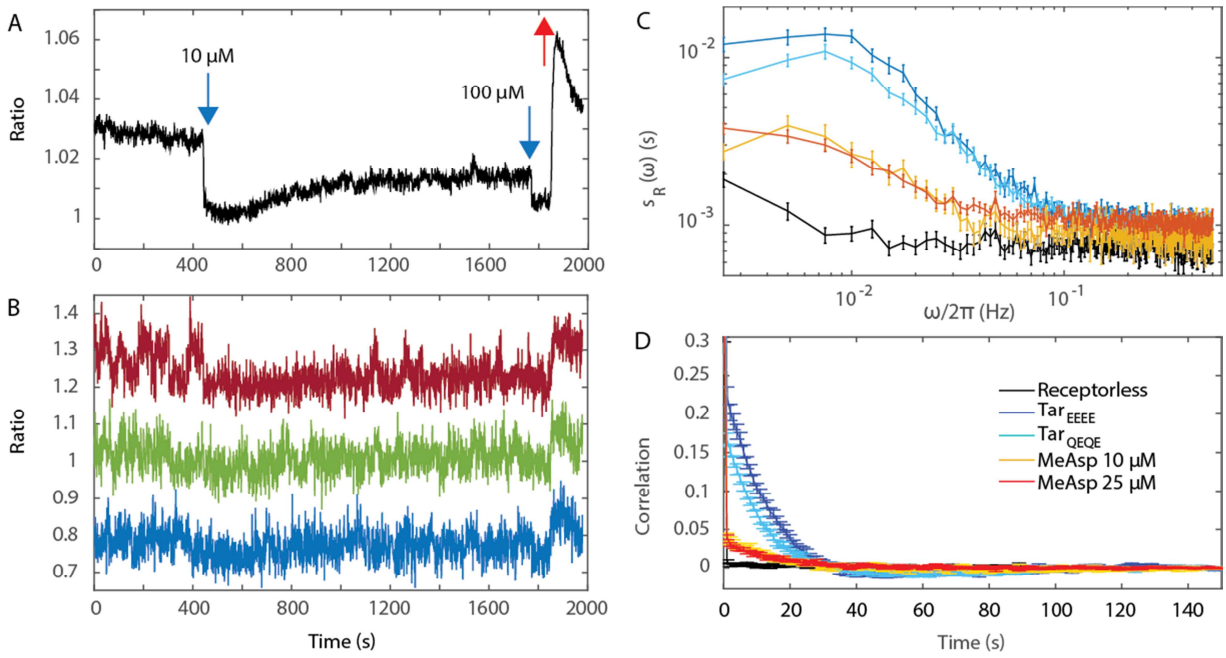

Figure 1. Single-cell measurements of the pathway activity in CheR$^+$ CheB$^+$ cells. (*A*) Time course of the population-averaged YFP/CFP ratio for the CheR$^+$ CheB$^+$ strain expressing the FRET pair CheY-YFP and CheZ-CFP and Tar as the sole receptor. Cells immobilized in a flow chamber under steady flow (see Materials and Methods) were initially adapted in buffer and subsequently stimulated by addition of indicated concentrations of a non-metabolizable chemoattractant MeAsp (blue arrows). The red arrow represents the removal of MeAsp. (*B*) Time course of the YFP/CFP ratio for representative single cells during the experiments depicted in (*A*). The measurement traces have been shifted along the y-axis to facilitate visualization. (*C*) Power spectral density (PSD) of the ratio measurements for single cells expressing Tar^{EEEE} or Tar^{QEQE} in buffer (dark and light blue curves) and Tar^{QEQE} cells adapted to 10 μM (orange curve) or 25 μM MeAsp (red curve), as well as for the receptorless strain in buffer (black curve). (*D*) The corresponding time autocorrelation functions of the single-cell ratio. The error bars represent standard errors (SEM), and the sample sizes are 103 (receptorless strain), 203 (Tar^{EEEE} in buffer), 265 (Tar^{QEQE} in buffer), 69 (10 μM) and 219 (25 μM) single cells coming from at least three biological repeats in each case.

Activity fluctuations in adaptation-deficient cells

We next tested whether the observed fluctuations could be solely explained by the action of the adaptation system, by measuring the single-cell pathway activity in a strain lacking CheR and

CheB. Given the observed dependence of the fluctuation on the level of the pathway activity, we first tested the Δ*cheRcheB* strain that was engineered to express Tar receptor in one-modified state (Tar^{QEEE}), which closely mimics the average modification state and intermediate activity of Tar in $CheR^+$ $CheB^+$ cells adapted in buffer [53, 59]. Expectedly, these cells showed a pronounced response but no adaptation to MeAsp, both at the population and single-cell level (Figure 2A). To our surprise, however, pathway activity in Tar^{QEEE} cells showed pronounced fluctuations despite the lack of adaptation system. In the strain expressing Tar^{QEQE} as the sole receptor, no fluctuations were observed in buffer, where Tar^{QEQE} is highly active and has low sensitivity to stimulation [59, 60]. Nevertheless, fluctuations were again observed when the activity of Tar^{QEQE} was partly inhibited by stimulating cells with an intermediate level of MeAsp (Figure 2B,C). In both cases, fluctuations were completely abolished upon saturating attractant stimulation, confirming their specificity.

Thus, at the intermediate level of pathway activity where the receptors are highly sensitive to stimulation, signaling fluctuations can be observed even in absence of the methylation system. Their PSD rose above shot noise at low frequency (roughly as $1/\omega$, see Figure 2C). Nevertheless, these methylation-independent fluctuations were slower than those observed in the $CheR^+$ $CheB^+$ strain (compare Figure 2C with Figure 1C), with a typical time scale of 34 ± 4 s (determined by single exponential fit of the curves of Figure 2D).

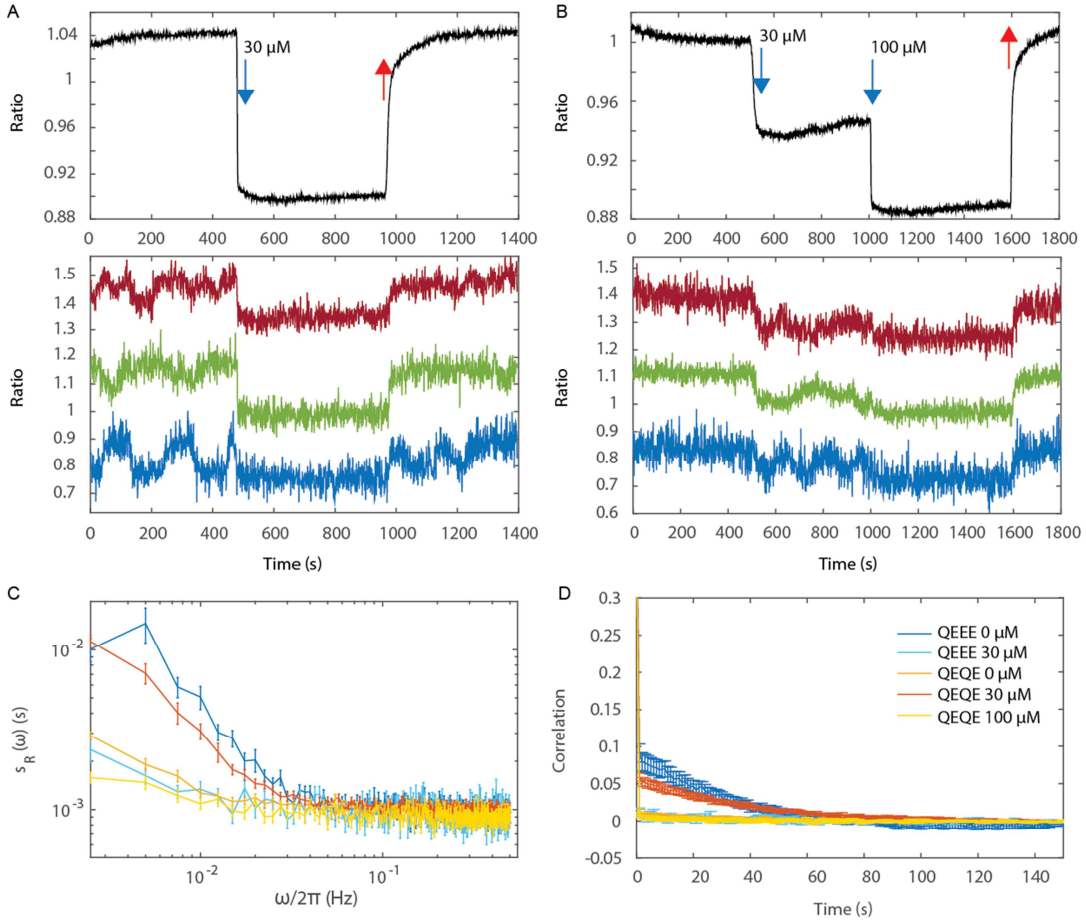

Figure 2. Pathway activity fluctuations in Δ*cheRcheB* cells. (*A*) Time course of the population-averaged (black) and typical single-cell (colors) YFP/CFP ratios for the Δ*cheR cheB* strain expressing Tar^{QEEE} as the sole receptor, in buffer and upon stimulation with 30 µM MeAsp, as indicated by the blue arrows. The red arrow represents the return to buffer condition. Measurements were performed as in Figure1. (*B*) Same as (A) but for the Δ*cheR cheB* strain expressing Tar^{QEQE} as the sole receptor and upon stimulation with 30 µM and then 100 µM MeAsp. (*C*) PSD of the single cell ratio for Tar^{QEEE} in buffer (blue) or in 30 µM MeAsp (cyan), Tar^{QEQE} in buffer (orange), in 30 µM MeAsp (red) or in 100 µM MeAsp (yellow). (*D*) Corresponding time autocorrelation functions of the single cell ratios. Error bars represent standard errors (SEM), and the sample sizes are 153 (Tar^{QEEE}, buffer), 65 (Tar^{QEEE}, 30 µM), 471 (Tar^{QEQE}, buffer), 404 (Tar^{QEQE}, 30 µM) and 136 (Tar^{QEQE}, 100 µM) single cells coming from at least three biological repeats in each case.

Role of receptor cooperativity in signaling noise

184 To investigate whether the observed fluctuations depend on cooperative interactions between
185 chemotaxis receptors, we utilized a recently described CheW-X2 version of the adaptor protein
186 CheW, which carries R117D and F122S amino acid replacements disrupting the formation of the
187 receptor arrays without abolishing signaling [61]. Indeed, a Δ*cheRcheB* strain expressing CheW-
188 X2 and Tar^{QEQE} showed basal activity and response to MeAsp which were similar to the
189 respective strain that has the native CheW (Figure 3A and Figure 3 – Figure Supplement 1).
190 Nevertheless, this strain showed no long-term fluctuations in the pathway activity, even when its
191 activity was tuned to an intermediate level (Figure 3B,C). Similarly, the array disruption allowed
192 signaling (Figure 3D) but abolished the long-term activity fluctuations in $CheR^{+}$ $CheB^{+}$ cells
193 (Figure 3E,F). These results demonstrate that long-term fluctuations in activity observed either
194 with or without the receptor methylation system require cooperative interactions between
195 receptors.
196

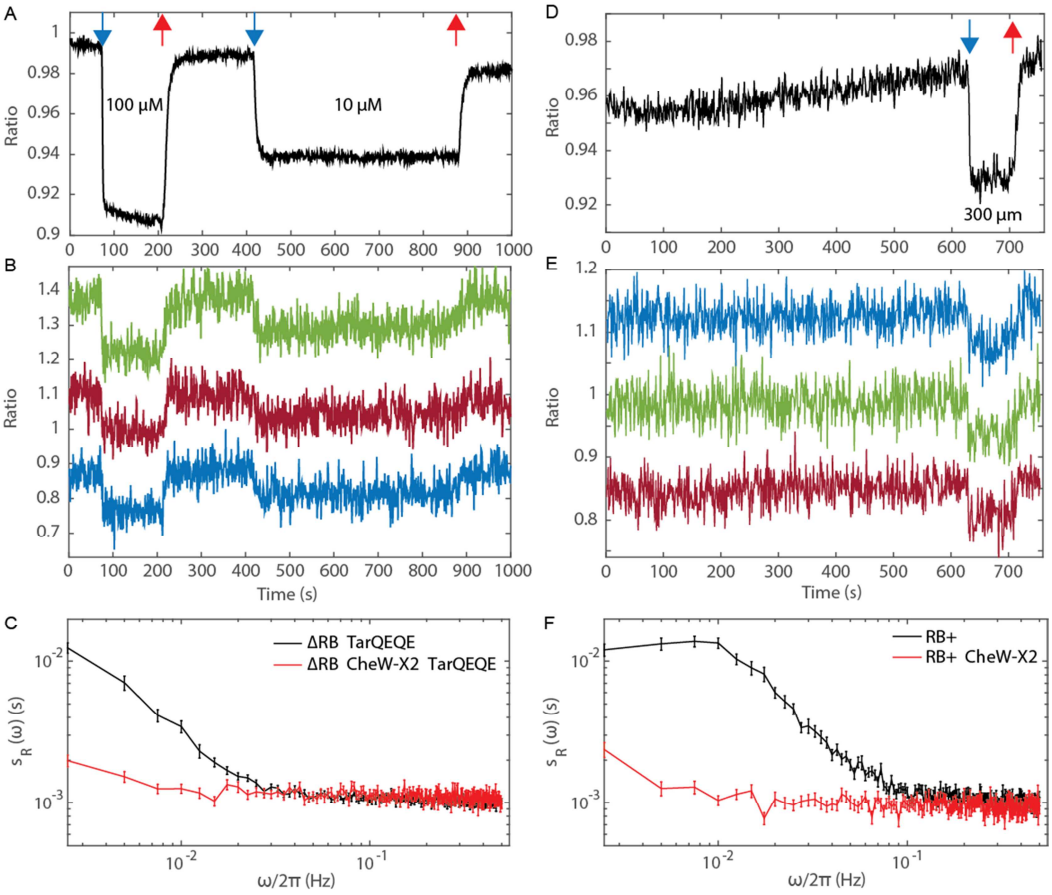

Figure 3. Fluctuation analysis in CheW-X2 cells. (*A*) Population averaged FRET ratio for adaptation deficient strain carrying CheW-X2 and Tar^{QEQE} as the sole receptor. The cells, which have a high activity in buffer, were first exposed to 100 µM MeAsp, which fully inhibited kinase activity, and then to 10 µM MeAsp to bring them to intermediate activity level. (*B*) Typical single cell FRET ratios for the same experiment as (A). The measurement traces have been shifted along the y-axis to facilitate visualization. (*C*) Power spectral density of the ratio fluctuations in CheW-X2 Δ*cheRcheB* strain (red) compared to the one in the equivalent strain carrying native CheW (black – same data as Figure 2C). Disruption of signal amplification through cooperativity eliminated the fluctuations. Error bars represent SEM, with sample sizes 404 (black) and 208 (red) cells. (*D-E*) Same as (A-B) in CheR^{+} CheB^{+} strain carrying CheW-X2 and Tar^{QEEE} as the sole receptor. The activity in buffer is intermediate level, 300 µM MeAsp completely inhibited the kinase activity. (*F*) Power spectral density of the ratio fluctuations in this strain (red) compared to the native CheW case (black – same data as Figure 1C with receptor Tar^{EEEE}). Error bars represent SEM, with sample sizes 202 (black) and 191 (red) cells. (*A-F*) Disruption of signal amplification through cooperativity eliminated the fluctuations.

211

212 **Fluctuation dissipation relation for receptor clusters**

213 To better understand the origin of the observed fluctuations and their relation to receptor
214 cooperativity, we considered the fluctuation dissipation theorem (FDT). It postulates that in
215 systems at equilibrium, thermal fluctuations of a quantity are related, via the temperature, to its
216 response to a small externally applied perturbation [62]. In out-of-equilibrium biological
217 systems, the process generating the fluctuations can be characterized by introducing an effective
218 temperature $T_{\mathrm{eff}}(\omega)$, which in this case describes the energy scale and frequency content of the
219 underlying out-of-equilibrium noise generating the fluctuations [63-66].

220 Such a fluctuation dissipation relation for the activity of a single receptor team can be used to
221 predict a relation between the PSD and the average FRET response to stimulation. We first
222 considered the simpler case of Δ*cheRcheB* cells, using an Ising-like model [51, 67, 68] to
223 describe cooperative receptor interactions in a team (see Material and Methods). For N_{teams}
224 signaling teams of strongly coupled signaling units in a cell, this yields:

225 $$s_R(\omega) = -2\,\frac{N\,T_{\mathrm{eff}}}{N_{teams}}\,\lambda^2\langle A\rangle(1-\langle A\rangle)\,\mathrm{Re}\big(\hat{\mathrm{g}}(\omega)\big) + \epsilon_0^2, \qquad (1)$$

226 where g is the normalized pathway response, N is the number of effective cooperative units in a
227 team, $\langle A\rangle$ is the average activity around which fluctuations occur, R is the YFP/CFP ratio, $R = \lambda A + \mu$ [54], and ϵ_0^2 is the measurement shot noise. Importantly, g could be experimentally
229 determined by measuring the FRET response to stepwise attractant stimulation as $g(t) = \Delta R(t)/\Delta R(+\infty)$ (Figure 4A). The values of λ could be estimated from experimental data (Figure
231 1A and 2A-B) as $\lambda_{RB-} \simeq 0.1$ and $\lambda_{RB+} \simeq 0.09$.

232 For Δ*cheRcheB* cells, we observed that $\mathrm{Re}\big(\hat{\mathrm{g}}(\omega)\big)$ – the real part of the Fourier transform of g –
233 was proportional to $s_R(\omega)$ for $\langle A\rangle \simeq 0.5$, at low frequencies (Figure 4B), as predicted by

Equation 1, also yielding the shot noise $\epsilon_0^2 \simeq 10^{-3}$. Furthermore, the PSD of these cells followed the scaling $\langle A\rangle(1-\langle A\rangle)$ predicted by the FDT, as evident for subpopulations of cells sorted according to their activity (Figure 4 – Figure Supplement 1). Thus, our model appears to accurately describe the observed long-time activity fluctuations in Δ*cheRcheB* cells, suggesting that these fluctuations could in principle be explained as the consequence of white noise driving an equilibrium system with the measured latency in the response to stimulation (Figure 4A). Notably, this latency in response has been previously observed and attributed to slow changes in packing of receptors within clusters [52]. Consistent with this interpretation, the CheW-X2 Δ*cheRcheB* strain with disrupted receptor clustering showed no response latency (Figure 3 – Figure Supplement 2) and no long-term activity fluctuations (Figure 3B,C).

Equation 1 further allowed us to estimate T_{eff}, the energy scale of the white noise driving activity fluctuations in the adaptation-deficient cells, which was nearly independent of ω (Figure 4D). For $\mathrm{Tar}^{\mathrm{QEQE}}$ at our expression level, $N \sim 14$ allosteric units [56, 59, 69, 70] yielded $kT_{\mathrm{eff}}/N_{teams} = 5.5\,10^{-3}kT$. To accurately count the number of signaling teams, the dose-response curve of Δ*cheRcheB* CheW-X2 expressing $\mathrm{Tar}^{\mathrm{QEQE}}$ (Figure 3 – Figure Supplement 1) was fitted using the MWC model, yielding a cooperativity number of N≃2. Since in this strain chemosensory complexes are believed to consist of two trimers of receptor dimers coupled to one CheA dimer [47, 61], this result suggests that N effectively accounts for the number of trimer of dimers (TD) in the signaling team. Assuming $N_{Tar} \sim 10^4$ receptor dimers under our induction level [42, 59], we obtain $N_{teams} = N_{Tar}/3N \simeq 240$ and $kT_{\mathrm{eff}} \sim 1.3\,kT$ (Figure 4D). Thus, thermal fluctuations coupled to the long-term dynamics of the receptor cluster should in principle be strong enough to generate the observed activity fluctuations.

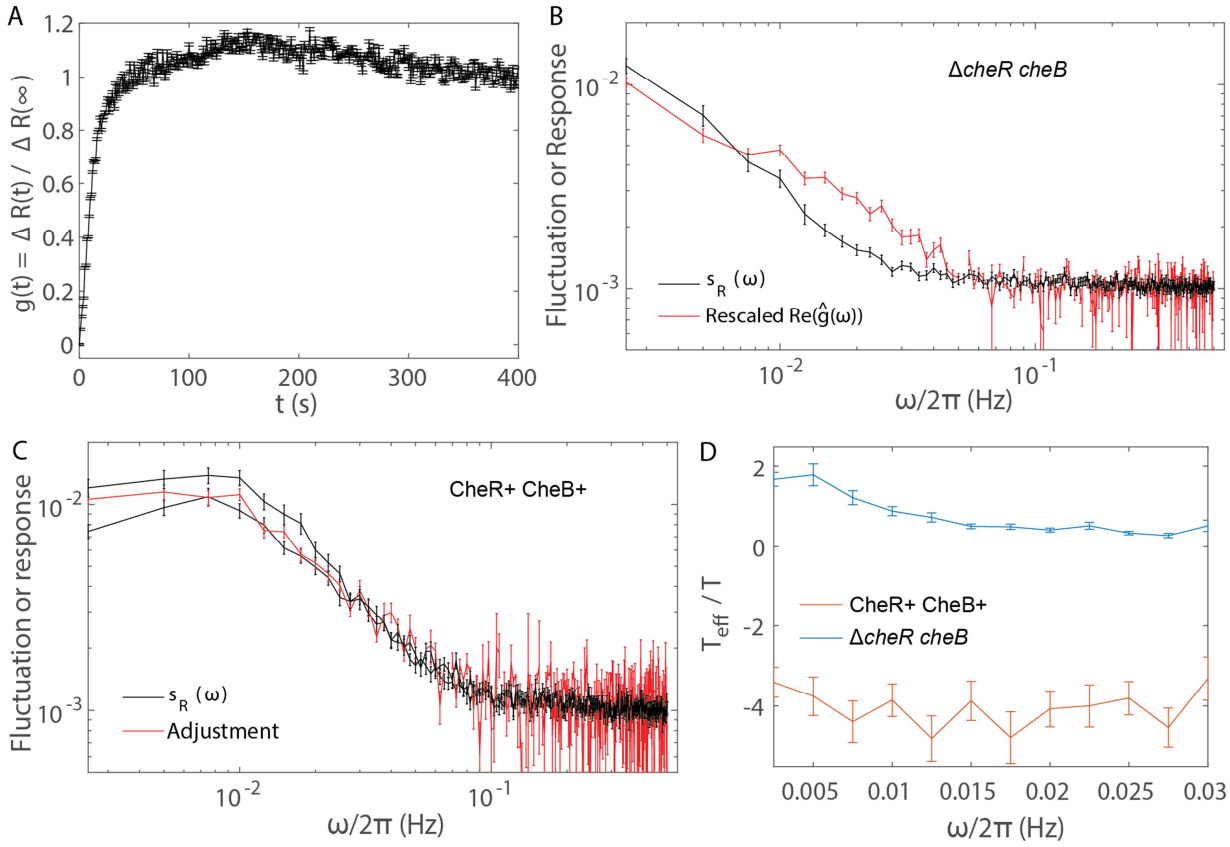

Figure 4. Fluctuation dissipation analysis of the pathway activity. (*A*) Normalized response function g(t) in the adaptation deficient case, evaluated in Δ*cheR cheB* + Tar^{QEQE} responding to a change from buffer condition to 30 μM MeAsp. (*B*) The PSD of the activity in adaptation deficient strains at activity $A = 0.5$ (black) was proportional to the response function in the frequency domain $\mathrm{Re}(\hat{g}(\omega))$ in the low frequency range, and adjusted to Eq. 1 (red). (*C*) The PSDs in adaptation proficient cells at $A = 0.5$ (black) were adjusted to Eq. 2, providing an estimate of the response function in adaptive cells (red). (*D*) Evaluated FDT ratios in both cases were constant, in the range of frequency where measurement noise is negligible. In all panels, error bars represent SEM, with sample sizes 540 (Δ*cheR cheB*) and 203 + 265 ($CheR^+$ $CheB^+$) single cells in at least 5 biological repeats.

Interestingly, we also observed that fluctuations were unaffected by the expression level of the receptors (Figure 4 – Figure Supplement 2). In the FDT framework, this would be the case only if $N/N_{teams} = 3N^2/N_{Tar}$ is constant. This indeed appears to agree with previous observation that the

cooperativity rises with expression level of Tar^{QEQE} in a way that N^2/N_{Tar} remains unchanged [59].

In presence of the adaptation enzymes, an effective fluctuation dissipation relation could be predicted in the same theoretical framework, additionally including adaptation described according to the classical two-state models of receptors [13, 69, 71], as

$$s_R^+(\omega) = 2k|T_{\text{eff}}|\frac{N\langle A\rangle(1-\langle A\rangle)}{N_{teams}}\ \lambda^2\ \frac{Re(\hat{g}(\omega))+\omega_{RB}\,|\hat{g}(\omega)|^2}{1+2\omega_{RB}\ Re(\hat{g}(\omega))+(\omega_{RB}|\hat{g}(\omega)|)^2}+\epsilon_0^2, \quad (2)$$

where $\omega_{RB} = N\langle A\rangle(1-\langle A\rangle)\,k_1(k_R + k_B(\langle A\rangle))$ is the activity-dependent rate of adaptation (see Material and Methods). The experimental $s_R(\omega)$ for $CheR^+$ $CheB^+$ cells was adjusted to Equation 2, using the function $\hat{g}(\omega)$ computed for *ΔcheRcheB*, the prefactor, ϵ_0^2 and ω_{RB} being adjustable parameters. The adjusted curve and the experimental PSD were in excellent agreement for the whole range of frequencies (Figure 4C). The estimated value of the methylation-dependent memory was $\tau_{RB} = 1/\omega_{RB} = 7.1\,s$, consistent with previous estimates [22], and the effective temperature was $kT_{\text{eff}} = -3.7\,kT$, assuming $\lambda = 0.09$ and other parameters as in the Δ*cheRcheB* case. We further considered that the adaptation enzymes are much fewer than their receptor substrates – only 15% of the receptors can be (de)methylated at any given time, since only 140 CheR and 240 CheB molecules [42] act on an assistance neighborhood of 7 and 5 receptor dimers respectively [43]. Given that the energy consumed by one methylation reaction is ΔH_m~30 kT [72], our estimate of the effective temperature in $CheR^+$ $CheB^+$ cells is consistent with random methylation events being the main driving force behind the activity fluctuations ($kT_{\text{eff}} - kT \simeq -0.15\Delta H_m$). Importantly, the sign of kT_{eff} for $CheR^+$ $CheB^+$ cells was negative, consistent with energy dissipation occurring during methylation-driven activity fluctuations [72-74]: Adaptation actively translates activity changes into receptor free energy gains – since (de)methylation events increase the energy of the receptors, before their

activity eventually actuates [74] – the opposite of the passive behavior of the receptors. This reversal of causality translates into a negative effective temperature on the time scales considered, where adaptation is the dominant cause of activity changes. Within our model, the loss of slow fluctuations upon disruption of clusters in $CheR^+$ $CheB^+$ cells (Figure 3F) could be easily explained by the dependence of $s_R(\omega)$ on the size N of signaling teams (Equation 2), meaning that reduction of N to 2 should largely abolish fluctuations in activity even in presence of the methylation system.

Discussion

The bacterial chemotaxis pathway has been extensively used as a model for quantitative analysis of signal transduction [10, 37, 46]. One fascinating feature of the chemotaxis pathway is the amplification of chemotactic signals through cooperative interactions within teams of clustered receptors, where ~10-20 receptor dimers show concerted transitions between active and inactive states [48-51, 75, 76]. Another much celebrated property of the pathway is robustness against external and internal perturbations, which largely relies on its methylation-based adaptation system [13, 14, 16, 40, 60]. At the same time, the stochastic activity of the adaptation enzymes was also proposed to induce variability in the signaling output on the time scale of tens of seconds [17, 18, 30], which might enhance environmental exploration [18, 23, 25, 27, 28].

Here we combine experimental and mathematical analyses to demonstrate that both, the adaptation system and receptor clustering contribute to the signaling noise in the chemotaxis pathway. Our single-cell FRET measurements reveal that large pathway activity fluctuations occur both in presence and in absence of the adaptation system, clearly showing that the

316 stochasticity of receptor methylation is not the sole cause of the pathway noise. The observed
317 fluctuations could be analyzed using the fluctuation dissipation theorem (FDT) and deviations
318 thereof. Multiple factors were accounted for, which apparently contribute to the overall pathway
319 noise: (i) an input white noise, (ii) the amplification of this noise by cooperative interactions
320 among receptors, (iii) the delayed response function of receptor clusters, and (iv) the dynamics of
321 the methylation system.
322 Our analysis suggests that, in adaptation deficient strains, the input noise likely originates from
323 thermal fluctuations of receptor activity, and it is converted into long-term pathway activity
324 fluctuations because of the latency observed in the response of clustered receptors. This observed
325 latency of response is consistent with the previous work that attributed it to changes in packing
326 of receptors within clusters [52]. Indeed, in our experiments it was abolished by mutations that
327 disrupt clustering. Notably, on the studied range of time scales the proposed contribution of the
328 high-frequency ligand binding noise [77] to overall fluctuations must be very small, since the
329 observed power spectral densities depended on activity but not on the absolute ligand
330 concentration. Our analysis also suggests that an effective subunit of the allosteric signaling
331 teams corresponds to one trimer of dimers, rather than a dimer itself as assumed in previous
332 computational models [59, 71]. This might be explained by the finite receptor-kinase coupling
333 within signaling teams, and it is consistent with a previous biochemical demonstration that a
334 trimer is necessary to activate CheA [78]. Notably, it could be easily reconciled with the
335 previous formulations of the MWC models by rescaling the free-energy change per methylated
336 glutamate by a factor of three.
337 In presence of the adaptation system this first source of noise seems to be added to the noise
338 coming from the stochasticity of methylation events. The adaptation system not only shifts the

frequency spectrum of fluctuations but also eliminates the latency of the response to stimuli, thus likely accelerating the response through its negative feedback activity. However, receptor clustering is required for the observed activity fluctuations even in presence of the adaptation system, likely because of signal amplification and accelerated adaptation dynamics within clusters [61]. Thus, although the receptor methylation system is clearly important for shaping the overall pathway noise, the resulting picture of the signaling noise in the native chemotaxis pathway is more complex than previously suggested. Altogether, our analysis shows that at least two sources of noise, with fairly comparable strengths, get first processed though a slow responding amplifier (the chemoreceptor cluster) and then fed back through the methylation system, resulting in complex colored fluctuations of the pathway activity and therefore of the swimming behavior.

More generally, our study provides another example of the general relation between fluctuations and response in biological systems [63-65, 79]. In these systems, the fluctuations are commonly shaped by active, non-equilibrium processes, the properties of which can be inferred from the deviations from the FDT. The approach of quantifying such deviations by means of an effective temperature, or fluctuation dissipation ratio, has been used in a variety of out-of-equilibrium systems [66], from glasses to biological systems. Although in some systems, *e.g.* glasses, this ratio can have indeed properties normally associated with the thermodynamic temperature, in biological systems it rather relates to the energy scale and frequency content of the underlying out-of-equilibrium processes, as demonstrated in the earing system [64] or in the active transport in eukaryotic cells [63, 65, 79]. For the chemotaxis pathway, our analysis indeed enabled us to distinguish between passive and active sources of noise, and also provided energy scale for the active process shaping the fluctuations that is well in agreement with the biochemical estimates.

Thus, fluctuation analyses may in general provide a valuable tool for studying cell signaling processes, from bacteria to mammals.

Material and Methods

Cell growth, media and sample preparation

E. coli strains and plasmids are described in Table S1 and Table S2, respectively. Cells carrying plasmids that encode indicated receptors and the FRET pair were grown at 30°C overnight in tryptone broth (TB) supplemented with appropriate antibiotics. The culture was subsequently diluted 17:1000 in TB containing antibiotics, 2 µM salicylate (unless otherwise stated) for induction of Tar and 200 µM isopropyl β-D-1-thiogalactopyranoside (IPTG) for induction of the FRET pair, and grown at 34°C under vigorous shaking (275 rpm) to an OD_{600} = 0.55. Bacteria were harvested by centrifugation, washed thrice in tethering buffer (10 mM KPO_4, 0.1 mM EDTA, 1 µM methionine, 10 mM lactic acid, pH 7) and stored at least 20 minutes at 4°C prior to the experiments.

Microscopy

Bacterial cells were attached to poly-lysine coated slides which were subsequently fixed at the bottom of a custom-made, air-tight flow chamber, which enables a constant flow of fresh tethering buffer using a syringe pump (Pump 11 Elite, Harvard Apparatus, Holliston, Massachusetts, United States) at 0.5 ml/min. This flow was further used to stimulate cells with indicated concentrations of α-methyl-D,L-aspartate (MeAsp). The cells were observed at 40x

magnification (NA = 0.95) using an automated inverted microscope (Nikon T*i* Eclipse, Nikon Instruments, Tokyo, Japan) controlled by the NIS-Elements AR software (Nikon Instruments). The cells were illuminated using a 436/20 nm filtered LED light (X-cite exacte, Lumen Dynamics, Mississauga, Canada), and images were continuously recorded at a rate of 1 frame per second in two spectral channels corresponding to CFP fluorescence (475/20 nm) and YFP fluorescence (542/27 nm) using an optosplit (OptoSplit II, CAIRN Research, Faversham, United Kingdom) and the Andor Ixon 897-X3 EMCCD camera (Andor Technology, Belfast, UK) with EM Gain 300 and exposure time of 1 s. For each measurement, the field of view was chosen to contain both a small region of high density with confluent cells and a few hundred well-separated single cells. During our approximately 30 min long measurements, the focus was maintained using the Nikon perfect focus system.

Image processing and data analysis

The image analysis was performed using the NIS-Elements AR software. The CFP and YFP images, each recorded by a half of the camera chip (256 x 512 px^2, 1 px = 0.40 µm), were aligned with each other by manual image registration. A gray average of the two channels was then delineated to enhance contrast and create binary masks with a user-defined, experiment-specific threshold. Individual cells were detected by segmentation of the thresholded image into individual objects, filtered according to size (3-50 $µm^2$) and shape (excentricity < 0.86). This step resulted in a collection of distinct regions of interest (ROIs) for each frame of the movie. The ROIs were then tracked from frame to frame, using the NIS build-in tracking algorithm. Only ROIs that could be tracked over the entire duration of the experiment were further analyzed. The selected ROIs were then inspected manually and those not representing individual

single cells well attached to the cover glass were discarded. Each individual measurement contained on the order of 100 tracked single cells.

All further analyses were carried out using MATLAB 8.4 R2014b (The MathWorks, Inc., Natick, Massachusetts, United States). For each tracked cell, the average CFP and YFP values over the ROI were extracted as a function of time. These values were also extracted for an ROI corresponding to the confluent population of cells. The ratio R of the YFP signal to the CFP signal was computed for both the single cells and the population, with the population response being used as a reference. Cells with a ratio change of less than 10% of the population response were discarded as unresponsive. The PSD was computed over T=400-frames long segments as

$$s_R(\omega) = \frac{1}{T}\left\langle \frac{\widehat{R_i}(\omega)\widehat{R_i}^*(\omega)}{\overline{R_i}^2} \right\rangle_i, \quad (3)$$

where $\widehat{R_i}(\omega)$ is the discrete Fourier transform of the ratio of cell i at frequency $\omega/2\pi$, $\widehat{R_i}^*$ its complex conjugate, $\overline{\cdot}$ represents a temporal average over the given time interval and $\langle\cdot\rangle_i$ an average over all single cells considered. The error for the PSD was evaluated as $\frac{1}{N_c T}\mathrm{var}\left(\frac{\widehat{R_i}(\omega)\widehat{R_i}^*(\omega)}{\overline{R_i}^2}\right)_i$, where N_c is the number of cells. The time autocorrelation function is simply the inverse Fourier transform of the PSD.

Modeling activity fluctuations in the framework of fluctuation dissipation relation

Ising model for the chemoreceptor cluster

The chemosensory complexes are described using an Ising model, in which the receptors can be in two states (OFF, which inhibits kinase, and ON, which actives kinase). The receptors and kinases are coupled, and the free energy difference between ON and OFF state is $\Delta f_0 = \gamma(m) + \eta(c)$ for a single receptor, with $\eta(c) = \ln\left(\left(1+\frac{c}{K_{OFF}}\right)/\left(1+\frac{c}{K_{ON}}\right)\right)$ being the contribution of

attractant binding and $\gamma(m) = k_0 - k_1 m$ being the contribution of the receptor methylation. The Hamiltonian of the whole sensory cluster is $H = H_{int} + \sum_{k=1}^{N_{Tar}} a_k \Delta f_0$, with a_k being the Boolean state of the receptor k and H_{int} describing the coupling between and among receptors and kinases. The interaction term H_{int} does not need to be specified for the following analysis, but it would be of the form $H_{int} = -J_{aa} \sum_{i,j}(A_i - 0.5)S_{i,j}(A_j - 0.5) - J_{ar} \sum_{i,k}(A_i - 0.5)V_{i,k}(a_k - 0.5) - J_{rr} \sum_{l,k}(a_l - 0.5)W_{l,k}(a_k - 0.5)$, where the J are the coupling strengths and S, V and W describe the network by determining whether two components are coupled and A_i is the Boolean activity of kinase i.

Phenomenological MWC description of the average response

Since analytical solutions for Ising models exist only in certain specific cases, an effective Monod-Wyman-Changeux (MWC) description of the system, extended to include the observed long-term response dynamics (see main text), was used to describe the average response of the system. The MWC model is known to well describe the pathway response, similarly to the Ising model [48, 50, 71, 80]. It considers that the cluster is divided in teams in which N allosteric units are coupled with infinite strength. Each team is then a two-state binary system, which can be either fully active or fully inactive. The probability of observing a team in the active state is given by $A = \frac{1}{1+\exp(N \Delta f_0)}$, with Δf_0 as above. The average methylation state of the team evolves under the action of CheR and CheB according to $\frac{dm}{dt} = k_R (1 - A) - k_B A$, with k_R and k_B being the rates of methylation and de-methylation, respectively [69]. In the classical MWC formulation, the basic subunit of the allosteric team is a receptor dimer. In contrast, our analysis suggests that, although N remains a measure of the extent of correlations, the allosteric subunits

rather consist of three dimers, which might be due to the actual finite coupling between the kinases and associated receptor dimers.

Phenomenological response function model for ΔcheRcheB cells

The dynamic susceptibility of the state of a single receptor $\chi_a(t)$ in response to a perturbation $+\epsilon$ of the free energy difference Δf_0 is defined as $\langle \delta a(t) \rangle = \int_{-\infty}^{t} -\epsilon(\tau)\, \chi_a(t-\tau)\, d\tau$, where $\langle \cdot \rangle$ is an ensemble average. In the case of a constant perturbation ϵ_0 starting at t = 0, $\langle \delta a(t) \rangle = -\epsilon_0 \int_0^t \chi_a(\tau)\, d\tau$. It is expected that $\langle \delta a(t) \rangle = \langle \delta A(t) \rangle$ on the time scales of our experiments. In the MWC framework, the same perturbation reduces the average activity by $\delta A_{MWC} = -N\, \langle A \rangle\, (1 - \langle A \rangle)\, \epsilon_0$, and $\chi_a(\tau)$ is then a delta function. In order to account for the long-term response dynamics observed in the experiments, we constructed a phenomenological model in which the activity can differ from the MWC expectation but evolves in time towards it, leading to a more complex form of $\chi_a(\tau)$. The MWC model was assumed to describe the static properties of the system, so that $\langle \delta a(+\infty) \rangle = \langle \delta A(+\infty) \rangle = \delta A_{MWC}$, which yields $\int_0^{+\infty} \chi_a(\tau)\, d\tau = N\langle A \rangle (1 - \langle A \rangle)$. We experimentally defined the function $g(t)$, measured as the response of a $\Delta cheRcheB$ strain to step-like attractant stimulation, as $g(t) = \Delta R(t)/\Delta R(+\infty) = \langle \delta A(t) \rangle / \langle \delta A(+\infty) \rangle$, which goes from 0 at $t = 0$ to 1 at $t = +\infty$.

The theoretical identification and the experimental definition were then combined to form the phenomenological model of the dynamic susceptibility of a receptor in the $\Delta cheRcheB$ strain as $\int_0^t \chi_a(\tau)\, d\tau = NA(1-A)g(t)$, which is expressed in Fourier space as

$$\hat{\chi}_a(\omega) = NA(1-A)i\omega\hat{g}(\omega) \qquad (4)$$

Here the Fourier transform of x is defined as

$$\hat{x}(\omega) = \int_{-\infty}^{+\infty} x(t) e^{-i\omega t}\, dt \tag{5}$$

473

474 ***Phenomenological response function model for CheR+ CheB+ cells***

475 We assumed that in presence of the adaptation system the receptor cluster responds to free
476 energy perturbations in the same way as in the adaptation-deficient cells, but this response
477 induces a methylation change adding up to the free energy perturbation. For a small sinusoidal
478 perturbation of the free energy difference $\epsilon(\omega)$, the resulting perturbations for the average
479 activity and methylation are then given in Fourier space by the set of equations

$$\langle \delta a(\omega) \rangle = NA(1-A) i\omega \hat{g}(\omega)(-\epsilon(\omega) + k_1 \langle \delta m(\omega) \rangle) \tag{6}$$

$$i\,\omega \langle \delta m \rangle = -(k_R + k_B) \langle \delta a(\omega) \rangle \tag{7}$$

480 Defining $\mathrm{X}_A^{\infty} = NA(1-A)$ and $\omega_{RB} = \mathrm{X}_A^{\infty} k_1 (k_R + k_B)$, this set of equations is easily solved
481 as

$$\langle \delta a(\omega) \rangle = \frac{\mathrm{X}_A^{\infty}\, i\omega\, \hat{g}(\omega)}{1 + \omega_{RB}\, \hat{g}(\omega)} \big(-\epsilon(\omega)\big) \tag{8}$$

482 We thus defined the dynamic susceptibility in this case as

$$\hat{\chi}_a^{+}(\omega) = \frac{\mathrm{X}_A^{\infty}\, i\omega\, \hat{g}(\omega)}{1 + \omega_{RB}\, \hat{g}(\omega)} \tag{9}$$

483 Note that the $\Delta cheRcheB$ case is obtained again if $\omega_{RB} = 0$.

484

485 ***Fluctuation dissipation relation***

486 For the allosteric chemosensory complexes described by the Ising model, the fluctuation
487 dissipation relation associated to the state a of a chemoreceptor is given by $s_a(\omega) =$

488 $-\frac{2\,kT}{\omega} Im\,\hat{\chi}_a(\omega)$, where $\hat{\chi}_a(\omega)$ is defined as above [62], assuming the system is in equilibrium.

489 The power spectral density of the state of the receptor is then

$$s_a(\omega) = -2\,kT\,\mathrm{Im}\left(\frac{\mathrm{X}_A^{\infty}\; i\;\hat{g}(\omega)}{1+\;\omega_{RB}\;\hat{g}(\omega)}\right)$$

$$= -2kT\;\mathrm{X}_A^{\infty}\;\frac{Re\big(\hat{g}(\omega)\big)+\;\omega_{RB}\;|\hat{g}(\omega)|^2}{1+2\;\omega_{RB}\;\;Re\big(\hat{g}(\omega)\big)+\;(\omega_{RB}|\hat{g}(\omega)|)^2} \qquad (7)$$

490 We then assumed that N_r neighboring receptors constitute a signaling team where all receptors
491 and associated kinases are in the same state (either OFF/inactive or ON/active) at a given time.
492 There are therefore $N_{teams} = N_{Tar}/N_r$ teams. The PSD of the average activity of the cell is
493 then $s_{A_{cell}}(\omega) = s_a(\omega)/N_{teams}$. This yields the PSD of the YFP/CFP ratio, the fluctuations of
494 which are proportional to the ones of A_{cell} with the factor λ, $s_R(\omega) = \lambda^2\, s_{A_{cell}}(\omega)$, leading to
495 equations 1 and 2, which also account for a constant value of ratio shot noise ϵ_0^2. In the case
496 where the origin of the noise is an out-of-equilibrium white noise, deviations to the equilibrium
497 FDT were quantified by introducing an effective temperature T_{eff}, normalized as the fluctuation
498 dissipation ratio T_{eff}/T, which characterizes the energy scale of the underlying noise in activity.
499 Note that although we expressed the fluctuation dissipation relation in terms of activity, which
500 allows us to directly compare the analysis with experimental data, this relation can be formulated
501 for any variable (e.g., receptor conformation) that itself determines the activity.
502
503 **Evaluation of λ**
504 In the non-adapting $\mathrm{Tar}^{\mathrm{QEQE}}$ strain, the value of λ_{RB-} was estimated as the difference, averaged
505 over all cells, between the YFP/CFP ratio in buffer, where the activity should be maximal (i.e.,
506 equal to one), and the ratio upon saturating stimulation with 100 µM MeAsp as $\lambda_{RB-} =$

$\langle \bar{R}\,(0)\rangle - \langle \bar{R}(100\,\mu M)\rangle$. In the adaptation-proficient strains, λ_{RB+} was evaluated as the difference between the ratio value during the brief stimulation with 100 µM MeAsp and the peak of the ratio upon removal of the stimulation (assuming that this value corresponds to maximal activity) averaging the ratio value over single cells.

Activity sorting

For Tar^{QEQE} receptors in non-adapting strains, we assumed that all the receptors are fully active in buffer conditions and fully inactive upon stimulation with 100 µM MeAsp. The pathway activity in each cell was thus evaluated as $A = 1 - \frac{\bar{R}(preStim-30\mu M) - \bar{R}(30\,\mu M)}{\bar{R}\,(preStim-100\,\mu M) - \bar{R}(100\,\mu M)}$. The use of the two different prestimulus values in buffer enables to minimize the effect of FRET baseline variation due to bleaching of fluorophores during image acquisition. Cells were then sorted according to their activity and divided into n equal subpopulations, and for each subpopulation the average PSD $\langle s_R(\omega)\rangle_A$ at average activity *A* of the subpopulation was evaluated for the set of frequencies displayed in Figure 4 – Figure Supplement 1. This procedure was implemented for several values of n, namely $n = 10, 9, 6, 5$ and 4, and the whole resulting data was used to plot $\langle s_R(\omega)\rangle_A$ as a function of *A*.

Acknowledgements

The authors would like to thank R. Somavanshi for assistance with experiments and N.S. Wingreen for comments on the manuscript.

Competing Interests

The authors declare no competing interests.

References

[1] ten Wolde P. R., Becker N. B., Ouldridge T. E. and Mugler A. *Fundamental Limits to Cellular Sensing.* Journal of Statistical Physics (2016) **162**, 1395, doi:10.1007/s10955-015-1440-5

[2] Rao C. V., Wolf D. M. and Arkin A. P. *Control, exploitation and tolerance of intracellular noise.* Nature (2002) **420**, 231, doi:10.1038/nature01258

[3] Tsimring L. S. *Noise in biology*. Reports on Progress in Physics (2014) **77**, doi:10.1088/0034-4885/77/2/026601

[4] Raj A. and van Oudenaarden A. *Nature, Nurture, or Chance: Stochastic Gene Expression and Its Consequences.* Cell (2008) **135**, 216, doi:10.1016/j.cell.2008.09.050

[5] Elowitz M. B., Levine A. J., Siggia E. D. and Swain P. S. *Stochastic gene expression in a single cell.* Science (2002) **297**, 1183, doi:10.1126/science.1070919

[6] Balazsi G., van Oudenaarden A. and Collins J. J. *Cellular Decision Making and Biological Noise: From Microbes to Mammals.* Cell (2011) **144**, 910, doi:10.1016/j.cell.2011.01.030

[7] Eldar A. and Elowitz M. B. *Functional roles for noise in genetic circuits.* Nature (2010) **467**, 167, doi:10.1038/nature09326

[8] Veening J. W., Smits W. K. and Kuipers O. P. *Bistability, Epigenetics, and Bet-Hedging in Bacteria.* Annual Review of Microbiology (2008) **62**, 193, doi:10.1146/annurev.micro.62.081307.163002

[9] Lan G. H. and Tu Y. H. *Information processing in bacteria: memory, computation, and statistical physics: a key issues review.* Reports on Progress in Physics (2016) **79**, doi:10.1088/0034-4885/79/5/052601

[10] Micali G. and Endres R. G. *Bacterial chemotaxis: information processing, thermodynamics, and behavior*. Current Opinion in Microbiology (2016) **30**, 8, doi:10.1016/j.mib.2015.12.001

[11] Levchenko A. and Nemenman I. *Cellular noise and information transmission.* Current Opinion in Biotechnology (2014) **28**, 156, doi:10.1016/j.copbio.2014.05.002

[12] Bowsher C. G. and Swain P. S. *Environmental sensing, information transfer, and cellular decision-making.* Current Opinion in Biotechnology (2014) **28**, 149, doi:10.1016/j.copbio.2014.04.010

[13] Barkai N. and Leibler S. *Robustness in simple biochemical networks.* Nature (1997) **387**, 913, doi:10.1038/43199

[14] Kollmann M., Lovdok L., Bartholome K., Timmer J. and Sourjik V. *Design principles of a bacterial signalling network.* Nature (2005) **438**, 504, doi:10.1038/nature04228

[15] Shinar G., Milo R., Martinez M. R. and Alon U. *Input-output robustness in simple bacterial signaling systems.* Proceedings of the National Academy of Sciences of the United States of America (2007) **104**, 19931, doi:10.1073/pnas.0706792104

[16] Alon U., Surette M. G., Barkai N. and Leibler S. *Robustness in bacterial chemotaxis.* Nature (1999) **397**, 168, doi:10.1038/16483

[17] Korobkova E., Emonet T., Vilar J. M. G., Shimizu T. S. and Cluzel P. *From molecular noise to behavioural variability in a single bacterium.* Nature (2004) **428**, 574, doi:10.1038/nature02404

[18] Emonet T. and Cluzel P. *Relationship between cellular response and behavioral variability in bacterial chernotaxis.* Proceedings of the National Academy of Sciences of the United States of America (2008) **105**, 3304, doi:10.1073/pnas.0705463105

[19] Berg H. C. and Brown D. A. *Chemotaxis in Escherichia-Coli Analyzed by 3-Dimensional Tracking.* Nature (1972) **239**, 500, doi:10.1038/239500a0

[20] Dufour Y. S., Gillet S., Frankel N. W., Weibel D. B. and Emonet T. *Direct Correlation between Motile Behavior and Protein Abundance in Single Cells.* Plos Computational Biology (2016) **12**, doi:10.1371/journal.pcbi.1005041

[21] Spudich J. L. and Koshland D. E., Jr. *Non-genetic individuality: chance in the single cell.* Nature (1976) **262**, 467, doi:10.1038/262467a0

[22] Park H., Pontius W., Guet C. C., Marko J. F., Emonet T. and Cluzel P. *Interdependence of behavioural variability and response to small stimuli in bacteria.* Nature (2010) **468**, 819, doi:10.1038/nature09551

[23] He R., Zhang R. J. and Yuan J. H. *Noise-Induced Increase of Sensitivity in Bacterial Chemotaxis.* Biophysical Journal (2016) **111**, 430, doi:10.1016/j.bpj.2016.06.013

[24] Viswanathan G. M., Buldyrev S. V., Havlin S., da Luz M. G. E., Raposo E. P. and Stanley H. E. *Optimizing the success of random searches.* Nature (1999) **401**, 911, doi:10.1038/44831

[25] Matthaus F., Jagodic M. and Dobnikar J. *E. coli Superdiffusion and Chemotaxis-Search Strategy, Precision, and Motility.* Biophysical Journal (2009) **97**, 946, doi:10.1016/j.bpj.2009.04.065

[26] Benichou O., Loverdo C., Moreau M. and Voituriez R. *Intermittent search strategies.* Reviews of Modern Physics (2011) **83**, doi:10.1103/RevModPhys.83.81

[27] Matthaus F., Mommer M. S., Curk T. and Dobnikar J. *On the Origin and Characteristics of Noise-Induced Levy Walks of E. Coli.* Plos One (2011) **6**, e18623, doi:10.1371/journal.pone.0018623

[28] Flores M., Shimizu T. S., ten Wolde P. R. and Tostevin F. *Signaling Noise Enhances Chemotactic Drift of E. coli.* Physical Review Letters (2012) **109**, 148101, doi:10.1103/PhysRevLett.109.148101

[29] Tu Y. and Grinstein G. *How white noise generates power-law switching in bacterial flagellar motors.* Physical review letters (2005) **94**, 208101, doi:10.1103/PhysRevLett.94.208101

[30] Pontius W., Sneddon M. W. and Emonet T. *Adaptation Dynamics in Densely Clustered Chemoreceptors.* Plos Computational Biology (2013) **9**, e1003230, doi:10.1371/journal.pcbi.1003230

[31] Springer M. S., Goy M. F. and Adler J. *Protein Methylation in Behavioral-Control Mechanisms and in Signal Transduction.* Nature (1979) **280**, 279, doi:10.1038/280279a0

[32] Goy M. F., Springer M. S. and Adler J. *Sensory Transduction in Escherichia-Coli - Role of a Protein Methylation Reaction in Sensory Adaptation.* Proceedings of the National Academy of Sciences of the United States of America (1977) **74**, 4964, doi:10.1073/pnas.74.11.4964

[33] Terwilliger T. C. and Koshland D. E. *Sites of Methyl Esterification and Deamination on the Aspartate Receptor Involved in Chemotaxis.* Journal of Biological Chemistry (1984) **259**, 7719,

[34] Kehry M. R. and Dahlquist F. W. *The Methyl-Accepting Chemotaxis Proteins of Escherichia-Coli - Identification of the Multiple Methylation Sites on Methyl-Accepting Chemotaxis Protein-I.* Journal of Biological Chemistry (1982) **257**, 378,

[35] Rice M. S. and Dahlquist F. W. *Sites of Deamidation and Methylation in Tsr, a Bacterial Chemotaxis Sensory Transducer.* Journal of Biological Chemistry (1991) **266**, 9746,

[36] Kehry M. R., Bond M. W., Hunkapiller M. W. and Dahlquist F. W. *Enzymatic Deamidation of Methyl-Accepting Chemotaxis Proteins in Escherichia-Coli Catalyzed by the Cheb Gene-Product.* Proceedings of the National Academy of Sciences of the United States of America (1983) **80**, 3599, doi:10.1073/pnas.80.12.3599

[37] Sourjik V. and Wingreen N. S. *Responding to chemical gradients: bacterial chemotaxis.* Current Opinion in Cell Biology (2012) **24**, 262, doi:10.1016/j.ceb.2011.11.008

[38] Hansen C. H., Endres R. G. and Wingreen N. S. *Chemotaxis in Escherichia coli: A Molecular Model for Robust Precise Adaptation.* PLoS Computational Biology (2008) **4**, e1, doi:10.1371/journal.pcbi.0040001

[39] Tu Y., Shimizu T. S. and Berg H. C. *Modeling the chemotactic response of Escherichia coli to time-varying stimuli.* Proceedings of the National Academy of Sciences of the United States of America (2008) **105**, 14855, doi:10.1073/pnas.0807569105

[40] Yi T. M., Huang Y., Simon M. I. and Doyle J. *Robust perfect adaptation in bacterial chemotaxis through integral feedback control.* Proceedings of the National Academy of Sciences of the United States of America (2000) **97**, 4649, doi:10.1073/pnas.97.9.4649

[41] Cluzel P., Surette M. and Leibler S. *An ultrasensitive bacterial motor revealed by monitoring signaling proteins in single cells.* Science (2000) **287**, 1652, doi:10.1126/science.287.5458.1652

[42] Li M. S. and Hazelbauer G. L. *Cellular stoichiometry of the components of the chemotaxis signaling complex.* Journal of Bacteriology (2004) **186**, 3687, doi:10.1128/Jb.186.12.3687-3694.2004

[43] Li M. S. and Hazelbauer G. L. *Adaptational assistance in clusters of bacterial chemoreceptors.* Molecular Microbiology (2005) **56**, 1617, doi:10.1111/j.1365-2958.2005.04641.x

[44] Schulmeister S., Ruttorf M., Thiem S., Kentner D., Lebiedz D. and Sourjik V. *Protein exchange dynamics at chemoreceptor clusters in Escherichia coli.* Proceedings of the

National Academy of Sciences of the United States of America (2008) **105**, 6403, doi:10.1073/pnas.071061110

[45] Taute K. M., Gude S., Tans S. J. and Shimizu T. S. *High-throughput 3D tracking of bacteria on a standard phase contrast microscope.* Nature Communication (2015) **6**, 8776, doi:10.1038/ncomms9776

[46] Tu Y. *Quantitative modeling of bacterial chemotaxis: signal amplification and accurate adaptation.* Annual Review of Biophysics (2013) **42**, 337, doi:10.1146/annurev-biophys-083012-130358

[47] Pinas G. E., Frank V., Vaknin A. and Parkinson J. S. *The source of high signal cooperativity in bacterial chemosensory arrays.* Proceedings of the National Academy of Sciences of the United States of America (2016) **113**, 3335, doi:10.1073/pnas.1600216113

[48] Mello B. A. and Tu Y. *Quantitative modeling of sensitivity in bacterial chemotaxis: the role of coupling among different chemoreceptor species.* Proceedings of the National Academy of Sciences of the United States of America (2003) **100**, 8223, doi:10.1073/pnas.1330839100

[49] Monod J., Wyman J. and Changeux J. P. *On Nature of Allosteric Transitions - a Plausible Model.* Journal of Molecular Biology (1965) **12**, 88, doi:10.1016/S0022-2836(65)80285-6

[50] Keymer J. E., Endres R. G., Skoge M., Meir Y. and Wingreen N. S. *Chemosensing in Escherichia coli: Two regimes of two-state receptors.* Proceedings of the National Academy of Sciences of the United States of America (2006) **103**, 1786, doi:10.1073/pnas.0507438103

[51] Duke T. A. J. and Bray D. *Heightened sensitivity of a lattice of membrane receptors.* Proceedings of the National Academy of Sciences of the United States of America (1999) **96**, 10104, doi:10.1073/pnas.96.18.10104

[52] Frank V. and Vaknin A. *Prolonged stimuli alter the bacterial chemosensory clusters.* Molecular Microbiology (2013) **88**, 634, doi:10.1111/mmi.12215

[53] Sourjik V. and Berg H. C. *Receptor sensitivity in bacterial chemotaxis.* Proceedings of the National Academy of Sciences of the United States of America (2002) **99**, 123, doi:10.1073/pnas.011589998

[54] Sourjik V., Vaknin A., Shimizu T. S. and Berg H. C. *In vivo measurement by FRET of pathway activity in bacterial chemotaxis.* Two-Component Signaling Systems, Pt B (2007) **423**, 365, doi:10.1016/S0076-6879(07)23017-4

[55] Meir Y., Jakovljevic V., Oleksiuk O., Sourjik V. and Wingreen N. S. *Precision and Kinetics of Adaptation in Bacterial Chemotaxis.* Biophysical Journal (2010) **99**, 2766, doi:10.1016/j.bpj.2010.08.051

[56] Neumann S., Vladimirov N., Krembel A. K., Wingreen N. S. and Sourjik V. *Imprecision of Adaptation in Escherichia coli Chemotaxis.* PLoS ONE (2014) **9**, e84904, doi:10.1371/journal.pone.0084904

[57] Krembel A. K., Neumann S. and Sourjik V. *Universal response-adaptation relation in bacterial chemotaxis.* Journal of Bacteriology (2014) JB.02171, doi:10.1128/JB.02171-14

[58] Berg H. C. and Tedesco P. M. *Transient-Response to Chemotactic Stimuli in Escherichia-Coli.* Proceedings of the National Academy of Sciences of the United States of America (1975) **72**, 3235, doi:10.1073/pnas.72.8.3235

[59] Endres R. G., Oleksiuk O., Hansen C. H., Meir Y., Sourjik V. and Wingreen N. S. *Variable sizes of Escherichia coli chemoreceptor signaling teams.* Molecular Systems Biology (2008) **4**, 211, doi:10.1038/Msb.2008.49

[60] Oleksiuk O., Jakovljevic V., Vladimirov N., Carvalho R., Paster E., Ryu W. S., Meir Y., Wingreen N. S., Kollmann M. and Sourjik V. *Thermal robustness of signaling in bacterial chemotaxis.* Cell (2011) **145**, 312, doi:10.1016/j.cell.2011.03.013

[61] Frank V., Pinas G. E., Cohen H., Parkinson J. S. and Vaknin A. *Networked Chemoreceptors Benefit Bacterial Chemotaxis Performance.* MBio (2016) **7**, doi:10.1128/mBio.01824-16

[62] Kubo R. *Fluctuation-Dissipation Theorem.* Reports on Progress in Physics (1966) **29**, 255, doi:10.1088/0034-4885/29/1/306

[63] Robert D., Nguyen T. H., Gallet F. and Wilhelm C. *In Vivo Determination of Fluctuating Forces during Endosome Trafficking Using a Combination of Active and Passive Microrheology.* Plos One (2010) **5**, e10046, doi:10.1371/journal.pone.0010046

[64] Martin P., Hudspeth A. J. and Julicher F. *Comparison of a hair bundle's spontaneous oscillations with its response to mechanical stimulation reveals the underlying active*

process. Proceedings of the National Academy of Sciences of the United States of America (2001) **98**, 14380, doi:DOI 10.1073/pnas.251530598

[65] Mizuno D., Tardin C., Schmidt C. F. and MacKintosh F. C. *Nonequilibrium mechanics of active cytoskeletal networks.* Science (2007) **315**, 370, doi:10.1126/science.1134404

[66] Cugliandolo L. F. *The effective temperature.* Journal of Physics a-Mathematical and Theoretical (2011) **44**, doi:10.1088/1751-8113/44/48/483001

[67] Hansen C. H., Sourjik V. and Wingreen N. S. *A dynamic-signaling-team model for chemotaxis receptors in Escherichia coli.* Proceedings of the National Academy of Sciences of the United States of America (2010) **107**, 17170, doi:10.1073/pnas.1005017107

[68] Shimizu T. S., Aksenov S. V. and Bray D. *A spatially extended stochastic model of the bacterial chemotaxis signalling pathway.* Journal of Molecular Biology (2003) **329**, 291, doi:10.1016/S0022-2836(03)00437-6

[69] Clausznitzer D., Oleksiuk O., Løvdok L., Sourjik V. and Endres R. G. *Chemotactic Response and Adaptation Dynamics in Escherichia coli.* PLoS Computational Biology (2010) **6**, e1000784, doi:10.1371/journal.pcbi.1000784

[70] Neumann S., Lovdok L., Bentele K., Meisig J., Ullner E., Paldy F. S., Sourjik V. and Kollmann M. *Exponential Signaling Gain at the Receptor Level Enhances Signal-to-Noise Ratio in Bacterial Chemotaxis.* Plos One (2014) **9**, doi:10.1371/journal.pone.0087815

[71] Mello B. A. and Tu Y. *Effects of adaptation in maintaining high sensitivity over a wide range of backgrounds for Escherichia coli chemotaxis.* Biophysical journal (2007) **92**, 2329, doi:10.1529/biophysj.106.097808

[72] Lan G., Sartori P., Neumann S., Sourjik V. and Tu Y. H. *The energy-speed-accuracy trade-off in sensory adaptation.* Nature Physics (2012) **8**, 422, doi:10.1038/Nphys2276

[73] Sartori P. and Tu Y. *Noise filtering strategies in adaptive biochemical signaling networks: Application to E. coli chemotaxis.* Journal of statistical physics (2011) **142**, 1206, doi:10.1007/s10955-011-0169-z

[74] Sartori P. and Tu Y. H. *Free Energy Cost of Reducing Noise while Maintaining a High Sensitivity.* Physical Review Letters (2015) **115**, doi:10.1103/PhysRevLett.115.118102

[75] Sourjik V. and Berg H. C. *Functional interactions between receptors in bacterial chemotaxis.* Nature (2004) **428**, 437, doi:10.1038/nature02406

[76] Li G. Y. and Weis R. M. *Covalent modification regulates ligand binding to receptor complexes in the chemosensory system of Escherichia coli.* Cell (2000) **100**, 357, doi:10.1016/S0092-8674(00)80671-6

[77] Aquino G., Clausznitzer D., Tollis S. and Endres R. G. *Optimal receptor-cluster size determined by intrinsic and extrinsic noise.* Physical Review E (2011) **83**, 021914, doi:10.1103/Physreve.83.021914

[78] Li M. S. and Hazelbauer G. L. *Selective allosteric coupling in core chemotaxis signaling complexes.* Proceedings of the National Academy of Sciences of the United States of America (2014) **111**, 15940, doi:10.1073/pnas.1415184111

[79] Chevry L., Colin R., Abou B. and Berret J. F. *Intracellular micro-rheology probed by micron-sized wires.* Biomaterials (2013) **34**, 6299, doi:10.1016/j.biomaterials.2013.05.002

[80] Skoge M. L., Endres R. G. and Wingreen N. S. *Receptor-receptor coupling in bacterial chemotaxis: Evidence for strongly coupled clusters.* Biophysical Journal (2006) **90**, 4317, doi:10.1529/biophysj.105.079905

[81] Neumann S., Grosse K. and Sourjik V. *Chemotactic signaling via carbohydrate phosphotransferase systems in Escherichia coli.* Proceedings of the National Academy of Sciences of the United States of America (2012) **109**, 12159, doi:10.1073/pnas.1205307109

[82] Krembel A., Colin R. and Sourjik V. *Importance of Multiple Methylation Sites in Escherichia coli Chemotaxis.* PLoS One (2015) **10**, e0145582, doi:10.1371/journal.pone.0145582

Supplementary Figures

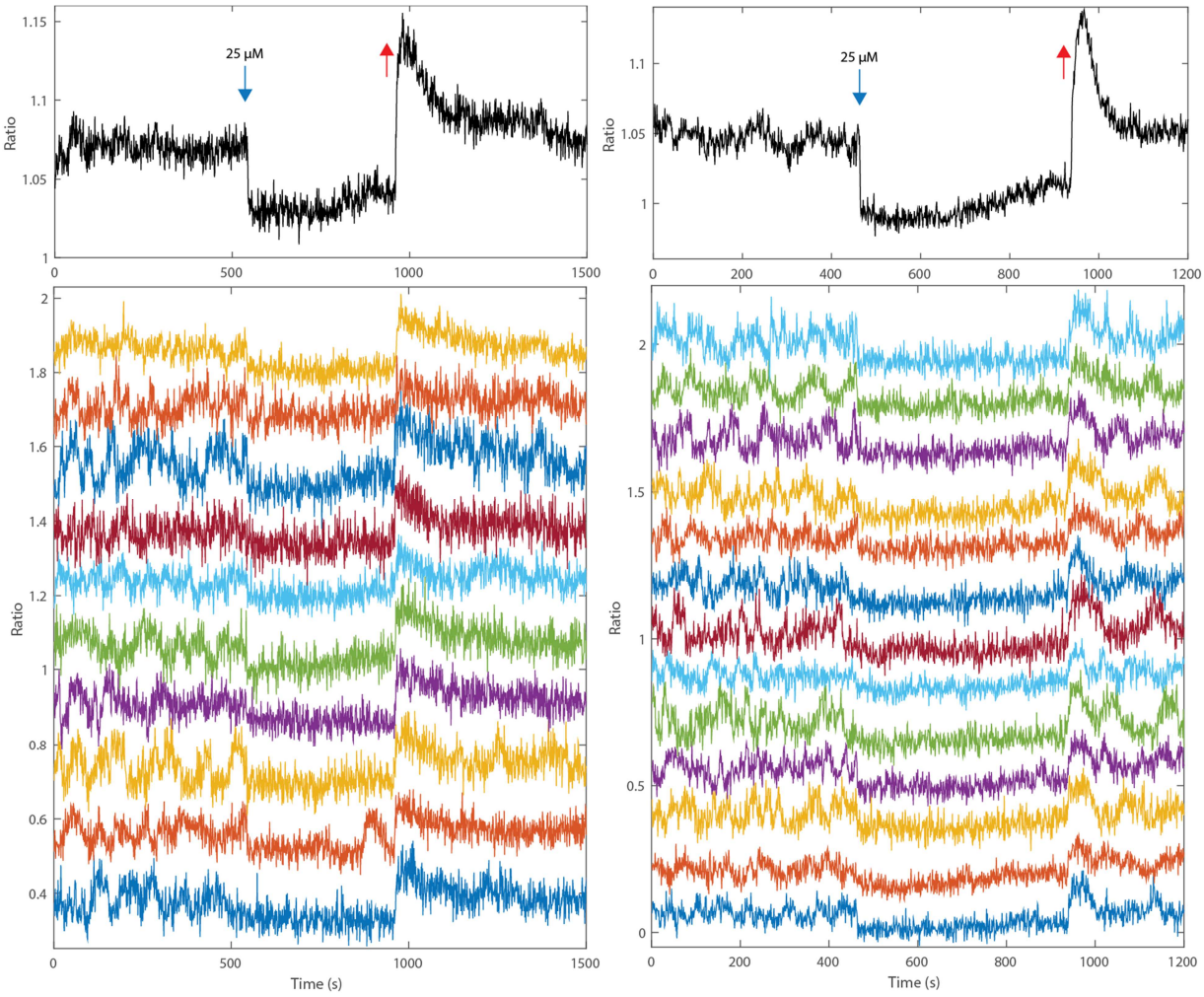

Figure 1 – Figure Supplement 1. Additional typical FRET ratios in adapting strain. Population averaged ratio (top) and corresponding single cell ratios (bottom), in two typical experiments, with adaptation proficient strain expressing Tar^{QEQE} as the sole receptor. Blue arrows indicate stimulation with 25 µM MeAsp, and red ones return to buffer condition. Ratios have been shifted to facilitate visualization.

780

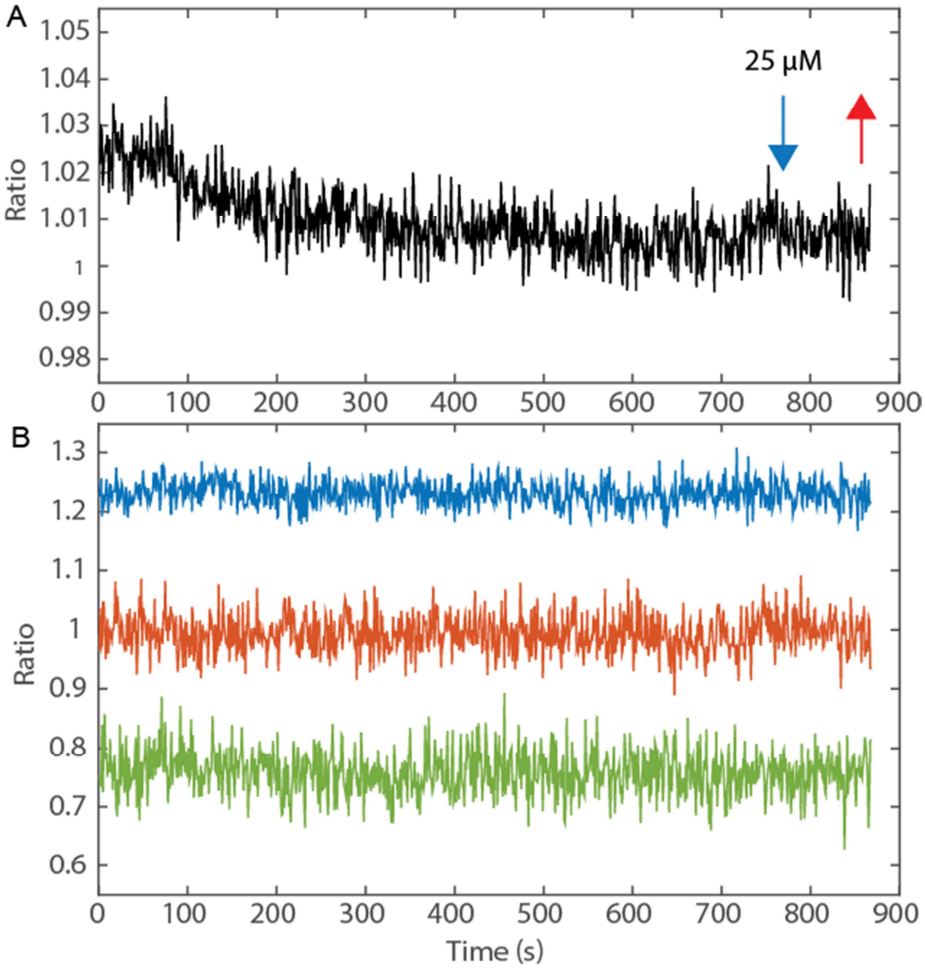

781

782 **Figure 1 – Figure Supplement 2. FRET ratios in the receptorless strain.** (*A*) Population
783 averaged ratio is mostly constant and exhibit no change in kinase activity upon stimulation with
784 25 μM MeAsp (arrow). (*B*) The single cell ratios were unresponsive and non-fluctuating. Only
785 shot noise, in a similar strength to the Tar positive strains, was observed.

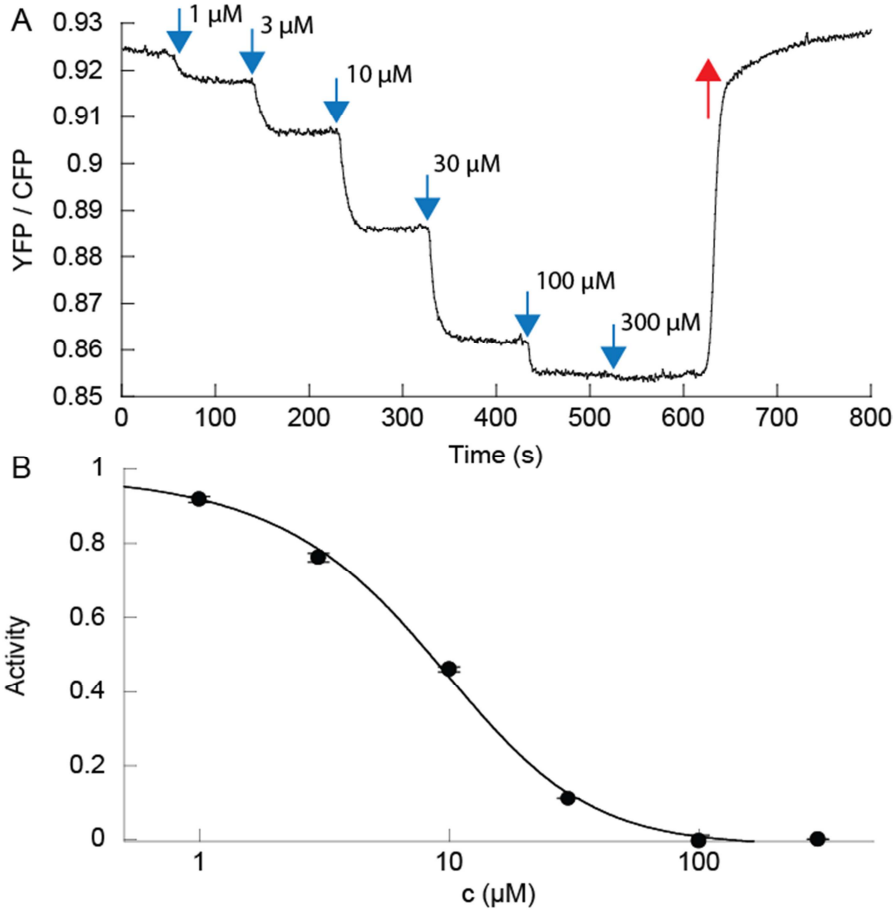

Figure 3 – Figure Supplement 1. Dose response to MeAsp of strain Δ*cheRcheB* CheW-X2 expressing Tar^{QEQE}. (*A*) Example of the YFP/CFP ratio (R) decreasing as increasing amounts of MeAsp were delivered to the cells. (*B*) The activity averaged over two biological replicates was estimated as $(R(c) - R_{min}) / (R_{max} - R_{min})$, plotted as a function of MeAsp concentration c, and fitted using the Monod-Wyman-Changeux model, assuming a free energy difference in absence of ligand $\gamma(m = 2) = -1$, yielding a cooperativity number N =1.73 and an inactive binding constant K_{OFF} = 3.92 µM. Fitting with a Hill function yields a Hill exponent H=1.4 and a concentration of half response EC_{50} = 8.3 µM. Error bars indicate SEM. Measurements were carried out on confluent populations of cells.

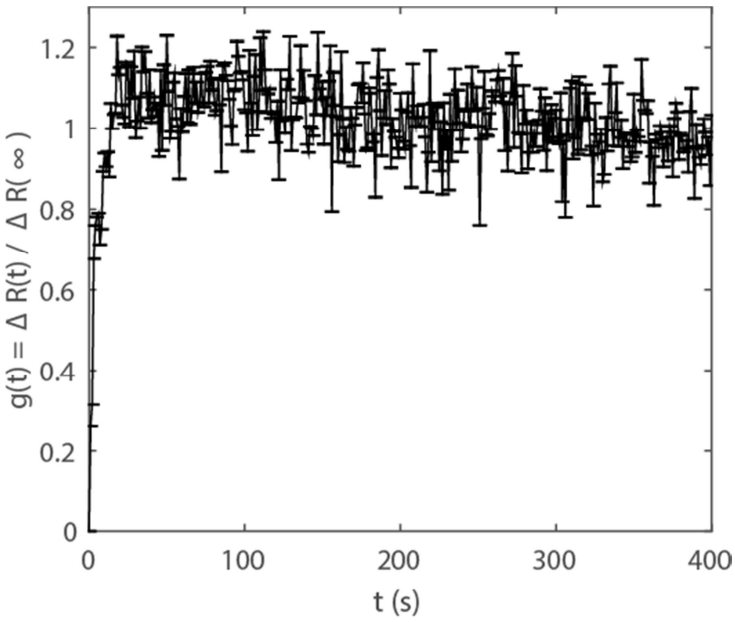

Figure 3 – Figure Supplement 2. Response function for the strain Δ*cheRcheB* CheW-X2 expressing Tar^{QEQE} as sole receptor. The strain was subjected to an increase of 10 µM MeAsp to measure the response. The long term dynamics observed in WT CheW strain is absent, the response being almost immediate (response time 4.5 ± 0.5 s, similar to the time necessary to achieve homogeneous concentration in the field of view). Error bars indicate SEM and sample size is 120 single cells, in 3 biological replicates.

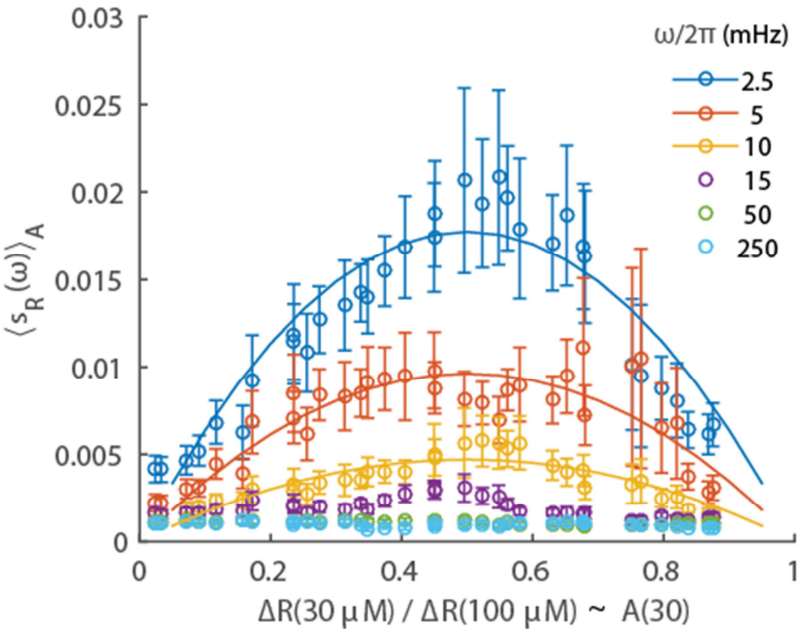

Figure 4 – Figure Supplement 1. Power spectral density computed on subsets of the cell populations sorted according to their activity, as a function of the average activity of the subsets, for the indicated frequencies (dots) in the Δ*cheRcheB* strain expressing Tar^{QEQE}. The lines correspond to best adjustments by $\langle s_R(\omega)\rangle_A = C(\omega)A(30)\big(1 - A(30)\big)$ for each frequency considered. The error bars correspond to SEM, sample sizes are as described in supplementary methods, varying from 54 to 135 cells depending on the point, taken from at least 5 biological replicates.

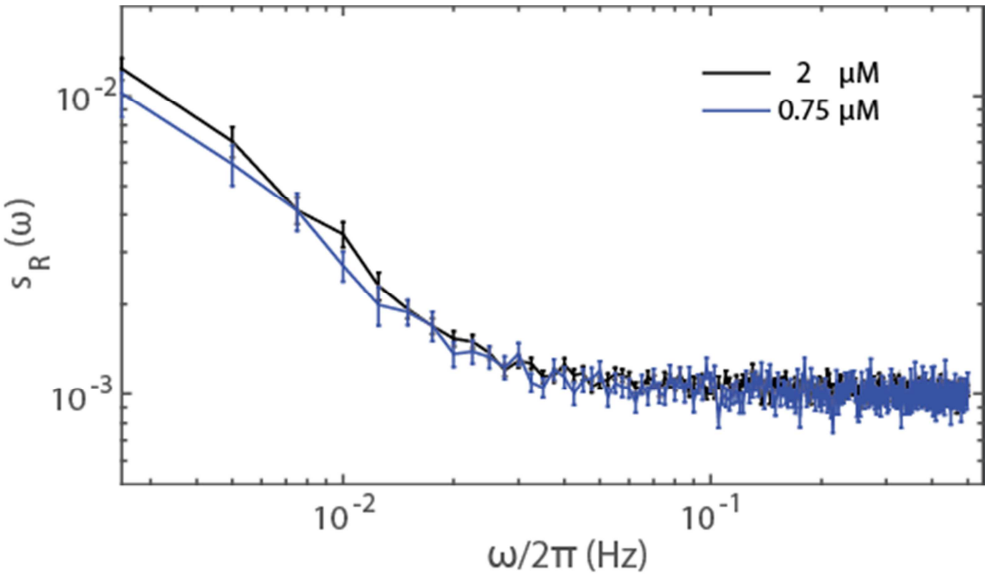

Figure 4 – Figure Supplement 2. Effect of the receptor expression level on the noise in non-adaptive strains. The Δ*cheR cheB* strain expressing Tar^{QEQE} as the sole receptor, from a plasmid under salicylate induction, was exposed to either 0.75 μM or 2 μM (standard experimental condition in the main text) salicylate, resulting in a factor of two between the protein numbers in the cell [59]. The power spectral density under 30 μM MeAsp, with average activity A =0.5, was the same in both conditions. Error bars indicate SEM and sample sizes are 540 (2 μM) or 187 (0.75 μM) cells.

827 **Supplementary Tables**

828 Table S1. Strain list

Strain	Genotype	Background	Ref.
VS181	Δ(tar,tsr,trg,tap,aer) Δ(cheY,cheZ)	RP437	[75]
VH1	Δ(tar,tsr,trg,tap,aer) Δ(cheY,cheZ) Δ(cheR,cheB)	RP437	[59]
VF7	Δ(tar,tsr,trg,tap,aer) Δ(cheY,cheZ) Δ(cheR,cheB) cheW(R117D,F122S)	RP437	[61]
VF8	Δ(tar,tsr,trg,tap,aer) Δ(cheY,cheZ) cheW(R117D,F122S)	RP437	[61]

829

830 Table S2. Plasmid list

Plasmid	Genotype	Antibiotic	Induction	Ref.
pVS88	cheY-YFP/cheZ-CFP, pTRC99a derivative	Ampicillin 100µg/ml	IPTG 200 µM,	[75]
pVS1092	Tar^{QEQE}, pKG110 derivative	Chloramphenicol 17 µg/ml	Salicylate 2 µM, If not otherwise stated	[75]
pVS1087	Tar^{QEEE}, pKG110 derivative	Chloramphenicol 17 µg/ml	Salicylate 2 µM, If not otherwise stated	[81]
pVS1086	Tar^{EEEE}, pKG110 derivative	Chloramphenicol 17 µg/ml	Salicylate 2 µM, If not otherwise stated	[82]

831

832